



Limited Archaean continental emergence reflected in an early Archaean ¹⁸O-enriched ocean

Benjamin W. Johnson ^{1,2} and Boswell A. Wing¹

The origin and evolution of Earth's biosphere were shaped by the physical and chemical histories of the oceans. Marine chemical sediments and altered oceanic crust preserve a geochemical record of these histories. Marine chemical sediments, for example, exhibit an increase in their $^{18}O/^{16}O$ ratio through time. The implications of this signal are ambiguous but are typically cast in terms of two endmember (but not mutually exclusive) scenarios. The oceans may have been much warmer in the deep past if they had an oxygen isotope composition similar to that of today. Alternatively, the nature of fluid-rock interactions (including the weathering processes associated with continental emergence) may have been different in the past, leading to an evolving oceanic oxygen isotope composition. Here we examine approximately 3.24-billion-year-old hydrothermally altered oceanic crust from the Panorama district in the Pilbara Craton of Western Australia as an alternative oxygen isotope archive to marine chemical sediments. We find that, at that time, seawater at Panorama had an oxygen isotope composition enriched in ^{18}O relative to the modern ocean with a $\delta^{18}O$ of $3.3 \pm 0.1\%$ VSMOW. We suggest that seawater $\delta^{18}O$ may have decreased through time, in contrast to the large increases seen in marine chemical sediments. To explain this possibility, we construct an oxygen isotope exchange model of the geologic water cycle, which suggests that the initiation of continental weathering in the late Archaean, between 3 and 2.5 billion years ago, would have drawn down an ^{18}O -enriched early Archaean ocean to $\delta^{18}O$ values similar to those of modern seawater. We conclude that Earth's water cycle may have gone through two separate phases of steady-state behaviour, before and after the emergence of the continents.

he physical and chemical histories of the oceans on Earth were critical determinants of the origin and evolution of Earth's biosphere. The oceans have mediated climatic feedbacks between the biosphere, atmosphere and geosphere through deep time, helping to ensure long-term planetary habitability. A tracer that integrates these dual aspects of oceanic history is the oxygen isotope composition of seawater. On geological timescales, the $\delta^{18}O$ value ($\delta^{18}O = [(^{18}O)^{16}O_{\text{sample}} - ^{18}O)^{16}O_{\text{VSMOW}}))^{18}O/^{16}O_{\text{VSMOW}}]$ of seawater, where VSMOW represents Vienna standard mean ocean water, an international standard that approximates the average oxygen isotope composition of modern ocean water) records the combined isotopic influences of hydrothermal alteration of oceanic crust (both high and low temperature), continental weathering, recycling efficiency of water and continental material at subduction zones, and any long-lived continental glaciers¹.

Although direct samples of ancient seawater are absent in records of the deep past, information on ancient ocean chemistry can be archived in the rock record. Two records, in particular, are thought to preserve seawater $\delta^{18}O$ in deep time: chemical sediments (for example, ref. 2) and altered oceanic crust (for example, ref. 3). The former record has been more thoroughly analysed, and includes carbonates, phosphates, microcrystalline silica and iron oxides. As these minerals form directly from aqueous species, they can reflect the $\delta^{18}O$ of the water with which they coexist. Measurements of oxygen isotope ratios in these sedimentary archives record a large secular increase through time $^{4-7}$, where older chemical sediments have lower $\delta^{18}O$ values that steadily increase through time to the present day.

This isotopic increase has typically been cast in terms of two endmember (but not mutually exclusive) interpretations: much higher past ocean temperatures with seawater δ^{18} O values buffered

near 0‰ through time^{5,8}; or more temperate seawater temperatures in the face of temporally evolving seawater δ¹⁸O values^{6,9,10}. An evolving oxygen isotope composition of seawater would indicate that the balance of isotopically distinct inputs and outputs of water to the ocean was different from that of the modern Earth. High-temperature fluid–rock interactions strip ¹⁶O from hydrothermal fluids, which isotopically enrich the ocean in ¹⁸O when these fluids are discharged at oceanic hydrothermal vents¹. Alternatively, low-temperature weathering on emergent continents and in shallow oceanic crust sequesters ¹⁸O away from the oceans¹. Secular variations in both processes have been proposed as a mechanism to evolve seawater δ¹⁸O over time^{6,9}.

Here we examine the record of the oxygen isotope composition of seawater preserved in altered oceanic crust^{1,11,12}. A long-standing body of knowledge provides strong evidence that the isotopic processes observed at modern mid-ocean ridge hydrothermal systems also occurred in the deep past^{3,11,13,14}. Minerals from the high-temperature portions^{15,16} of ancient oceanic hydrothermal systems record the δ^{18} O values of the local hydrothermal fluid, suggesting that isotopic exchange between fluid and rock approaches equilibrium conditions in settings with closely spaced fracture networks¹⁷.

We build on these realizations and present a new inverse method that interprets two-dimensional oxygen isotope patterns in oceanic crustal rocks representing both the low-temperature, shallow portions of hydrothermal systems and the high-temperature portions hosted in deep crust. A unique aspect of this approach is that we impose both local and system-wide mass balance to each setting, focusing on how the process of local fluid-mediated oxygen isotope exchange naturally scales up to a consistent spatial pattern of ¹⁸O enrichments and depletions when viewed over an entire hydrothermal system ¹⁸. We confirm this method against oxygen isotope

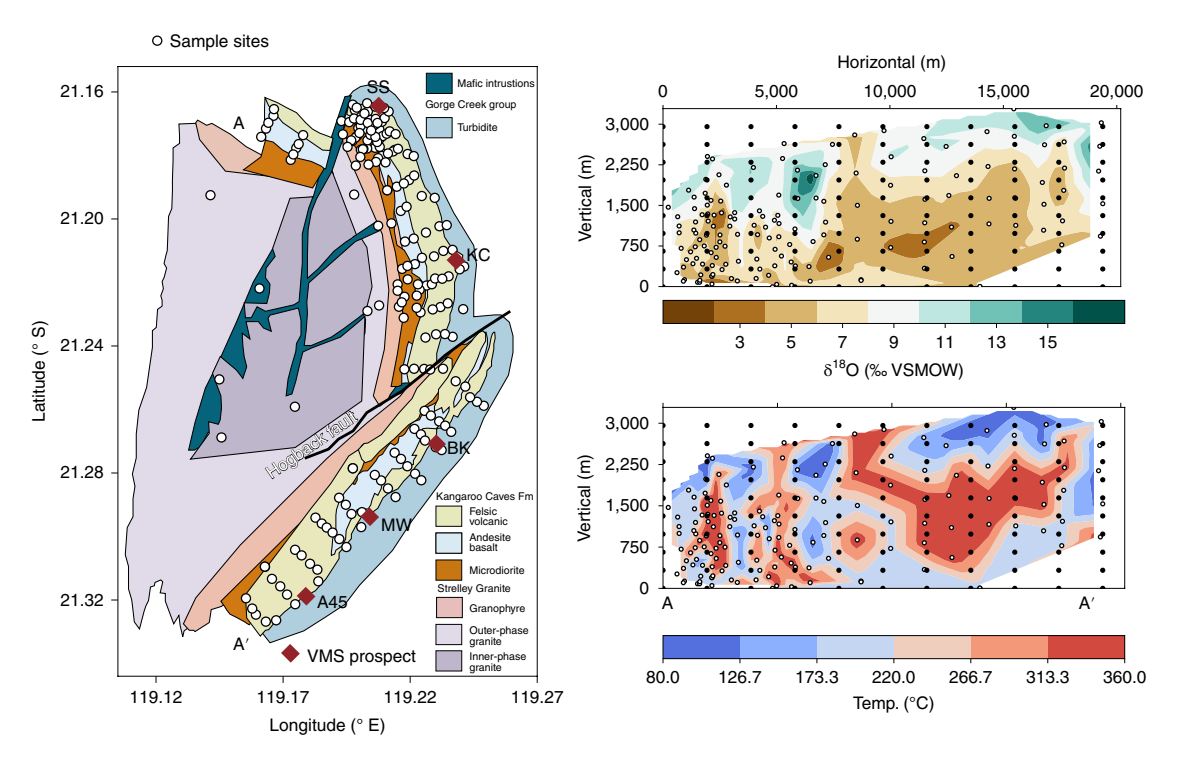


Fig. 1 | Simplified geologic map and reconstructed temperature and oxygen isotope cross-sections of the Panorama District. Left: a geologic map³⁷ overlain with sample sites for oxygen isotope determination. Whole-rock oxygen isotope measurements are from Ni-bomb fluorination⁴⁰. The VMS prospects (red diamonds) are the inferred discharge zones of hydrothermal cells: Sulphur Springs (SS), Kangaroo Caves (KC), Breakers (BK), Man O' War (MW) and Anomaly 45 (A45). Right: the reconstructed oxygen isotope and temperature cross-sections go from north (A) on the left to south (A') on the right, and start from the base of the volcanic pile. The white dots in all panels represent sample sites, and the black dots in the right-hand subplots are the corners of the grid boxes used in the data inversion.

cross-sections from Mesozoic and Cenozoic oceanic crust, and then exploit the exquisitely exposed fossil hydrothermal system found in the 3.24-Gyr-old Panorama volcanogenic massive sulfide (VMS) district, Pilbara, Australia (Fig. 1). By targeting Palaeoarchaean oceanic crust, we focus on a time period where hypotheses for steady-state and evolving seawater δ^{18} O are characterized by their largest differences (0% (ref. 5) and -9% (for example, ref. 9)).

Inverse model, calibration, benchmarking and confirmation

We adapt a tracer mass-balance inversion approach from the ocean circulation literature¹⁹ that has been used previously in geochemical studies of crustal fluid flow^{20,21}. The technique relies on whole-rock oxygen isotope measurements and independent estimates of alteration temperatures, with the goal of inverting these local data to sum the total amount of fluid that altered a given body of rock. Given this estimated fluid/rock ratio for the entire hydrothermal system, as well as average system-wide isotopic and thermal properties, we then solve for the δ^{18} O of the fluid feeding the entire flow system²².

We calibrated the smoothing parameter that is required to produce a unique solution by inverting a synthetic dataset of isotopic patterns and temperature²¹. This study²¹ developed an analytical model for equilibrium oxygen isotope exchange between oceanic crust with a constant initial δ^{18} O and infiltrating seawater of 0%, under a hydrothermal system driven by a two-dimensional temperature profile that was fixed in time. It is therefore an exact forward representation of isotopic alteration under the governing assumptions in our inverse model. We imposed a starting rock δ^{18} O of 5.7%0 and sampled these forward model results (their Fig. 1) to tune the smoothing parameter in our inversions. A value of 2.05×10^{-4} reproduced the imposed infiltrating seawater of 0%0 (see Methods and Extended Data Fig. 1).

To benchmark the inverse model, we inverted a synthetic oxygen isotope and temperature dataset from another forward model (their Fig. 21)²³, holding constant the calibrated smoothing parameter. This model numerically described the isotopic consequences of hydrothermal seawater–ocean crust interactions under kinetic, rather than equilibrium, isotope exchange, as well as a time-dependent thermal evolution of the hydrothermal system. We chose to invert results that represent the full duration of the model calculation to examine the impact of these assumptions over the entire lifetime of a hydrothermal system. In spite of these different forward model conditions, our inversion still reproduces the incoming fluid value of $\sim 0\%$ ($-0.5\pm0.1\%$; Extended Data Fig. 1) imposed in the forward model, given a starting rock δ^{18} O of 7.5% (ref. 23). This establishes the second-order isotopic influence of kinetics, especially at temperatures >100 °C (ref. 23).

Finally, we also benchmarked the inverse model against a simulation of the coupled oxygen isotope and temperature evolution associated with the hydrothermal alteration of the Skaergaard intrusion (their Fig. 24)¹⁸. This system was fed by freshwater²⁴, and the modelled incoming fluid in ref. ¹⁸ had a δ^{18} O value of -14%c. We held constant the calibrated smoothing parameter in this case as well, and returned an inverse estimate within error of the imposed of δ^{18} O for the infiltrating fluid ($-14.5\pm0.9\%c$; Extended Data Fig. 1), assuming a starting δ^{18} O value for plagioclase of 7%c (ref. ¹⁸). This benchmark illustrates that the inverse approach can distinguish internal redistribution of oxygen isotopes from whole-system variations driven by changes in the δ^{18} O values of external fluids.

To confirm our inverse approach, we applied it to oxygen isotope and temperature records from three fossil Cenozoic–Mesozoic oceanic hydrothermal systems: the 0.2-Myr-old Hess Deep exposure of the East Pacific Rise²⁵; the 14.2-Myr-old Fukazawa–Kosaka area²⁶;

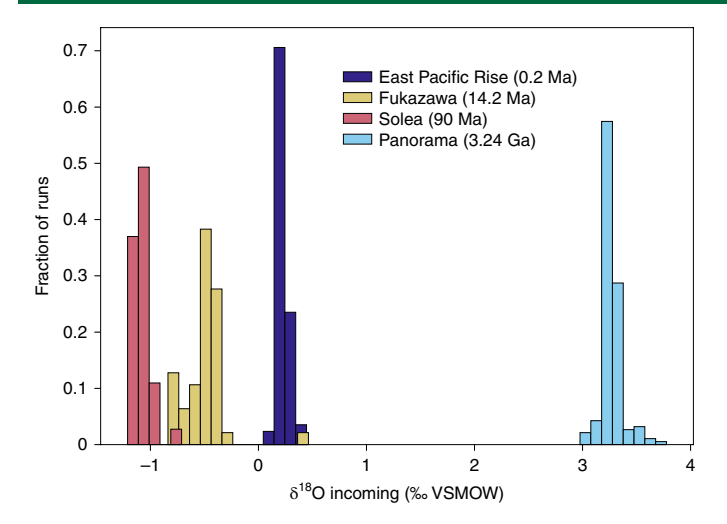


Fig. 2 | Results of 'leave-one-out' inversions, removing one sample each time from each dataset and re-running the entire inverse procedure. Each set of inversions has the same number of runs as there are samples in each dataset (Supplementary Table 2).

and the 91.6 \pm 1.4-Myr-old Solea Graben in the Troodos ophiolite^{27,28} (Fig. 2 and Supplementary Fig. 3). For all three times, the δ^{18} O of seawater has been independently estimated from Mg/Ca and δ^{18} O analyses of benthic foraminifera²⁹ at 0.2%, about -0.5% and -1%, respectively (Fig. 3).

These three systems represent a diversity of spreading centres, from mid-ocean ridges to back-arc basins, and they have each experienced fluid-rock interaction of different duration and intensity. This is evident in the fluid/rock ratios estimated for each site (Extended Data Fig. 2), as well as the range seen in each site's δ^{18} O data (Extended Data Fig. 3). Despite these differences, the inverse method returned incoming seawater δ^{18} O values that match well with what has been proposed for the latest Mesozoic and Cenozoic²⁹ (inset of Fig. 3). We take these results to mean that the smoothing parameter calibrated on the initial synthetic dataset is suitable for use in natural settings. In addition, it appears that any isotopic ageing that may occur after the hydrothermal system dies out but before the crustal section is exposed, including any alteration associated with obduction, does not impact the inverse results. Finally, the ability to distinguish the relatively small isotopic variations proposed for Cenozoic-Mesozoic seawater suggests that we will be able to discriminate between the much larger isotopic differences that characterize hypotheses for the δ^{18} O of Palaeoarchaean seawater.

An exceptional exposure of 3.24-Gyr-old oceanic crust

The Panorama VMS district of the Pilbara Craton in northern Western Australia preserves a 3,238±3-Myr-old section of oceanic crust³⁰⁻³². There are two broad hypotheses for the geologic setting at Panorama. The first suggests that the area was formed as a series of volcanic plateaux, with sporadic underplating and proto-subduction³³. The second suggests modern-like horizontal plate tectonics, with spreading centres and subduction zones (for example, ref. ³⁴). Regardless of exact setting, there is ample evidence that the Panorama district formed in a submarine setting and interacted hydrothermally with infiltrating seawater.

The 3–4-km-thick Panorama volcanic pile is represented by the Kangaroo Caves Formation, and ranges in composition from basalt to dacite, with minor components of rhyolite (Fig. 1). There are abundant pillow basalts, as well as an exhalative chert horizon, at the top of the pile indicating preservation of the palaeoseafloor. Very shortly after the formation of the volcanic pile,

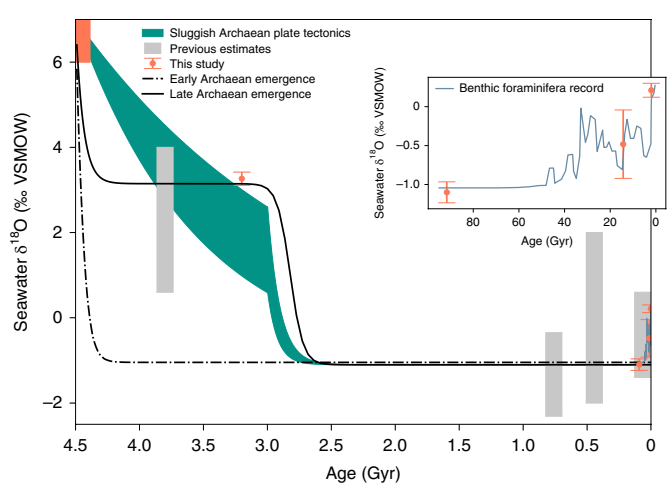


Fig. 3 | Calculated seawater δ^{18} O evolution for different rate efficiency and continental emergence scenarios. Previous estimates for seawater δ^{18} O from submarine basalts (from oldest to youngest: ref. 41, ref. 16, ref. 12, ref. 15 and ref. 25) are shown in grey boxes, with our results shown as orange dots (error bars represent two standard deviations). Note the youngest grey box combines two estimates of Phanerozoic seawater δ^{18} O. The constraint at 4.45 Ga (orange box) is based on basaltic magma-water equilibrium^{1,42,43} and a bulk Earth $\delta^{18}O = 5.5\%$. The inset shows estimated seawater $\delta^{18}O$ for the Cenozoic and the latest Mesozoic based on benthic foraminiferal oxygen isotopes and Mg/Ca ratios²⁹. The green field indicates sluggish Archaean plate tectonics, which are defined by water cycling at 2-4% of modern rates that increase to modern values at 3 Ga. The dot-dash line indicates establishment of continental water cycling in the early Archaean while the solid line indicates establishment in the late Archaean. This plot highlights that there are no constraints on seawater δ^{18} O during the Proterozoic eon from oceanic crustal rocks, so we assumed that $\delta^{18}O$ of Proterozoic seawater resembled Phanerozoic seawater.

it was intruded by the Strelley Granite, which is indistinguishable in age $(3,239\pm2\,\mathrm{Myr}$ old) from the volcanics³². This intrusion slightly tilted the volcanic strata and drove a series of five distinct hydrothermal cells now demarcated by VMS prospects at Sulphur Springs, Kangaroo Caves, Breakers, Anomaly 45 and Man O' War³¹. Although there were three main stages of deformation regionally³⁵, the Panorama strata were rotated as a near-solid body and experienced low strain throughout their post-formation history³⁶. The completeness of the Panorama section, as evidenced by preservation of palaeo-seafloor down to the granitic heat engine, makes it an ideal quantitative record of hydrothermal alteration in Palaeoarchaean oceanic crust³¹,³⁶-³ී.

Alteration of the volcanic rocks at Panorama by downwelling seawater is preserved both mineralogically and geochemically^{31,38}. The alteration patterns reflect broad low-temperature recharge zones separated by more narrow high-temperature discharge zones capped by massive sulfide mounds³¹. In the recharge zones, the initial mineralogy has been altered to a feldspar-sericitequartz assemblage, while in the discharge zones it is now primarily chlorite-quartz³¹. The alteration patterns are further defined as maps of fluid-mobile elements (for example, Cu, Mo, Zn), which were stripped from wall rocks in regions of up-temperature fluid flow and precipitated in sulfide mounds at discharge sites^{37,38}. Fluid inclusions record seawater infiltration into the volcanic pile during a single phase of hydrothermal activity, and insignificant input of magmatic water³⁹. The temperatures estimated from fluid inclusions correlate closely with alteration mineral assemblages³⁹; thus, we assigned a temperature of alteration to each sample based on their associated mineral zone³¹ (Fig. 1).

In addition to geochemical, mineralogical and thermal evidence for Panorama's hydrothermal history, there is a well-resolved record of whole-rock oxygen isotope alteration across the entire district⁴⁰ (Fig. 1) The oxygen isotope patterns at Panorama, with higher δ^{18} O values near the palaeo-seafloor and lower values at depth are similar to profiles of more recent altered oceanic crust^{3,25} and ophiolites¹³. These similar system-wide oxygen isotope patterns through time reflect an overall calculable balance between ¹⁸O depletion in the deep crust through high-temperature fluid-rock interactions and ¹⁸O enrichment in the shallow crust through low-temperature alteration.

Applying our inverse model to the Panorama system returns a $\delta^{18}\text{O}$ value for incoming seawater at 3.24 Gyr ago (Ga) of $3.3 \pm 0.1\%$ VSMOW (Fig. 2). This is about 4% enriched compared to a modern, ice-free ocean, and contrasts strongly with previously proposed values of 0% (ref. 5) and -9% (for example, ref. 9) for the Palaeoarchaean ocean. The system-scale fluid/rock ratio from the inversion, however, is within the range of those estimated for the East Pacific Rise, Solea and Fukazawa (Extended Data Fig. 2), potentially indicating broadly similar driving forces for hydrothermal fluid flow in oceanic crustal environments through time.

Seawater oxygen isotope history from oceanic crustal rocks

When viewed in a temporal perspective, the seawater δ^{18} O history implied by oceanic crustal rocks differs markedly, in sign and magnitude, from the record inferred from chemical sediments. In addition to the results reported here, an ¹⁸O-enriched ocean has been identified at 3.8 Ga, with a δ^{18} O value ranging from +0.8 to +3.8% ϵ (ref. 41), while estimates for more recent times (late Neoproterozoic into the Phanerozoic) centre around a δ^{18} O value of about -1%(Fig. 3). This apparent long-lived pattern is also consistent with predictions of a primordial ocean δ^{18} O value of +6 to +8%o (refs. ^{1,42,43}). Isotopic equilibrium with a basaltic melt of $\delta^{18}O = +5.5\%$ (ref. 44) at temperatures expected for the waning stages of a magma ocean after the Moon-forming impact (1,200–1,300 °C; ref. 45) could produce such ¹⁸O-enriched water. A quasi-exponential decay from these high original values is a natural consequence of the fact that the magnitude of oxygen isotope exchange processes that control seawater δ^{18} O depend on seawater δ^{18} O itself^{1,43,46}.

Here we take advantage of a published kinetic model for the change in oceanic δ^{18} O with time⁴³ (see Supplementary Information) and a quantitative synthesis of modern ¹⁸O exchange between the hydrosphere and geosphere¹ to ask: whether time-invariant oxygen cycling can lead to the broad patterns of oceanic δ^{18} O through time; and, if not, whether minimal changes to the structure or magnitude of the ¹⁸O-enabled water cycle can reproduce these patterns. We modified slightly the published net fractionation factor (Δ_{cw}) associated with continental weathering to produce an ice-free ocean δ^{18} O value of -1%0 while using directly the rates of oxygen cycling (k_i) between the hydrosphere and solid Earth reservoirs as well as other Δ_i values (Supplementary Table 1).

Although modern rates and fractionation factors result in an ^{18}O -enriched ocean declining to a modern-like steady-state $\delta^{18}\text{O}$ value (Fig. 3), the timescale for this change is much too short to yield an ^{18}O -enriched ocean in the Palaeoarchaean. This is a direct consequence of the rapidity of oxygen cycling on modern Earth, which processes about an ocean's worth of oxygen every $\sim 40\,\text{Myr}$ ($\sum k_i = 26.1\,\text{Gyr}^{-1}$; Supplementary Table 1). A stepped exponential decay model can fit observations of a secular decrease in seawater $\delta^{18}\text{O}$ through time (Fig. 3), however, as long as the overall magnitude of the rate of oxygen cycling is $\sim 2-4\%$ as efficient as modern ($\sum k_i = 0.5 - 1.0\,\text{Gyr}^{-1}$) at the start of the Archaean eon, increasing to modern levels by $\sim 2.5\,\text{Ga}$ (Extended Data Fig. 5). Such oxygen cycling implies sluggish plate tectonics relative to the modern for much of the Archaean. There are geophysical and geochemical hypotheses consistent with plate tectonics at this time

(for example, ref. ⁴⁷) and, if the fluid/rock ratios calculated for the Panorama VMS district relative to more recent Fukazawa VMS district (Extended Data Fig. 2) are representative, Palaeoarchaean oceanic heat flux may have indeed been less than Miocene heat flux. Application of the technique reported here to other sections of Archaean and Proterozoic oceanic crust may enable evaluation of this possibility.

A decrease in seawater δ^{18} O from >3% to -1% can also be reproduced by simple structural changes in the kinetic model, without modifying rates from their modern values (Supplementary Table 1 and Extended Data Fig. 4). The ¹⁸O-enriched Palaeoarchaean ocean identified here can be reproduced if the early Archaean water cycle was characterized purely by oceanic oxygen cycling (low-temperature and high-temperature exchange with submarine basalts; water recycling through the mantle), while continental oxygen isotope cycling only 'turned on' sometime after ~3.2 Ga (Fig. 3). In addition to oceanic oxygen exchange rates at their modern values, this alternative also requires a distinct early Archaean fractionation factor associated with high-temperature hydrothermal alteration of oceanic crust of 1.4% that evolves to its modern value of 4.1% after 3 Ga (Supplementary Table 1). In this model, the ocean evolves quickly from an initially high δ^{18} O value (7%) to a steady state of about 3%, and then, as continental weathering and recycling rise from zero to modern rates by ~2.5 Ga, the isotopic steady state is lowered to the modern ice-free δ^{18} O value of -1%. Although emergent continental blocks have been identified as early as ~3.5 Ga (ref. ⁴⁸), the seawater δ^{18} O record does not appear to record their influence on global-scale continental weathering and recycling of sediments into continental crust. Cratonscale exposure surfaces, however, are present in the ~3-Gyr-old Pongola Basin⁴⁹ and recent work on the ¹⁷O record in shales suggests widespread subaerial weathering of continental crust by about ~2.5 Ga (ref. 50).

Both of these simple oxygen isotope evolution models imply limited continental emergence for much of the Archaean. As a result, we can estimate the size of important continental reservoirs as continental oxygen isotope cycling is initiated. The Archaean ocean mass is estimated to be 1 to 1.7 times larger than the modern one $(1.21 \times 10^{21} \text{ to } 2.1 \times 10^{21} \text{ kg})^{41,51}$, which means that evolution of seawater δ^{18} O from 3% to -1% would require removal of between 6×10^{17} and 1.0×10^{18} mol of ¹⁸O. If sediments were the ultimate sink for this oxygen, assuming a δ¹⁸O of 12.7% (ref. ⁵⁰) and approximating sediments as 70% kaolinite (Al₂Si₂O₅(OH)₄) and 30% quartz (SiO₂), the isotopic shift implies development of a sedimentary reservoir that is between 4×10^{20} and 7×10^{20} kg. This is between 22 and 34% of the mass of the modern sedimentary shell⁵². Using the same approach for continental crust, but given a δ^{18} O of 7.8% (ref. 53) and approximating the crust as granitic with a chemical formula of KAlSi₃O₈, indicates nascent weatherable continents of 7×10^{20} to 1.1×10^{21} kg (3–5% modern⁵²). We stress that these are minimum estimates, as they represent the amount of oxygen that must be exchanged to shift oceanic δ^{18} O from 3%e to -1%e. Growth of more crustal or sedimentary mass is certainly possible, especially given recent evidence for an even more 18O-depleted early Proterozoic ocean than assumed here7.

We recognize that these quantitative narratives for continental emergence are not unique. They do, however, underscore that growth of an ^{18}O -enriched surface reservoir is necessary to drive Palaeoarchaean oceanic $\delta^{18}\text{O}$ to less positive values more characteristic of modern times. The emergence of continents, the initiation of subaerial weathering, and the formation of a granite-rich crust and clay-rich sedimentary shell provide a consilient solution to this situation. Whether these emergent processes happened slowly or rapidly, in the late Archaean or in the Protoerozic, are all open questions that can be answered with the new approach described here. An early Earth without emergent continents may have resembled

a 'water world', providing an important environmental constraint on the origin and evolution of life on Earth⁵⁴ as well as its possible existence elsewhere⁵⁵.

Online content

Any methods, additional references, Nature Research reporting summaries, source data, extended data, supplementary information, acknowledgements, peer review information; details of author contributions and competing interests; and statements of data and code availability are available at https://doi.org/10.1038/s41561-020-0538-9.

Received: 7 January 2019; Accepted: 13 January 2020; Published online: 2 March 2020

References

- Muehlenbachs, K. The oxygen isotopic composition of the oceans, sediments and the seafloor. Chem. Geol. 145, 263–273 (1998).
- Prokoph, A., Shields, G. & Veizer, J. Compilation and time-series analysis of a marine carbonate δ¹⁸O, δ¹³C, ⁸⁷Sr/⁸⁶Sr and δ³⁴S database through Earth history. Earth Sci. Rev. 87, 113–133 (2008).
- Muehlenbachs, K. & Clayton, R. Oxygen isotope composition of the oceanic crust and its bearing on seawater. J. Geophys. Res. 81, 4365–4369 (1976).
- Chase, C. & Perry, E. C. The oceans: growth and oxygen isotope evolution. Science 177, 992–994 (1973).
- Knauth, L. P. & Lowe, D. R. High Archean climatic temperature inferred from oxygen isotope geochemistry of cherts in the 3.5 Ga Swaziland Supergroup, South Africa. Geol. Soc. Am. Bull. 115, 566–580 (2003).
- Jafrés, J. B., Shields, G. A. & Wallmann, K. The oxygen isotope evolution of seawater: a critical review of a long-standing controversy and an improved geological water cycle model for the past 3.4 billion years. *Earth Sci. Rev.* 83, 83–122 (2007).
- Galili, N. et al. The geologic history of seawater oxygen isotopes from marine iron oxides. Science 365, 469–473 (2019).
- Garcia, A. K., Schopf, J. W., Yokobori, S.-i, Akanuma, S. & Yamagishi, A. Reconstructed ancestral enzymes suggest long-term cooling of Earth's photic zone since the Archean. *Proc. Natl Acad. Sci. USA* 114, 4619–4624 (2017).
- Kasting, J. F. et al. Paleoclimates, ocean depth, and the oxygen isotopic composition of seawater. Earth Planet. Sci. Lett. 252, 82–93 (2006).
- Veizer, J. & Prokoph, A. Temperatures and oxygen isotopic composition of Phanerozoic oceans. Earth Sci. Rev. 146, 92–104 (2015).
- 11. Muehlenbachs, K. & Clayton, R. N. Oxygen isotope studies of fresh and weathered submarine basalts. *Can. J. Earth Sci.* **9**, 172–184 (1972).
- 12. Muehlenbachs, K., Furnes, H., Fonneland, H. C. & Hellevang, B. Ophiolites as faithful records of the oxygen isotope ratio of ancient seawater: the Solund-Stavfjord Ophiolite Complex as a Late Ordovician example. *Ophiolites Earth Hist.* **218**, 401–414 (2003).
- Gregory, R. T. & Taylor, H. P. Jr An oxygen isotope profile in a section of Cretaceous oceanic crust, Samail Ophiolite, Oman: evidence for δ¹⁸O buffering of the oceans by deep (>5 km) seawater-hydrothermal circulation at mid-ocean ridges. *J. Geophys. Res. Solid Earth* 86, 2737–2755 (1981).
- Gregory, R. T. in Ophiolites in Earth History Vol. 218 (eds Dilek, Y. & Robinson, P. T.) 353–368 (Geological Society, 2003).
- Turchyn, A. V. et al. Reconstructing the oxygen isotope composition of late Cambrian and Cretaceous hydrothermal vent fluid. *Geochim. Cosmochim.* Acta 123, 440–458 (2013).
- Hodel, F. et al. Fossil black smoker yields oxygen isotopic composition of neoproterozoic seawater. Nat. Commun. 9, 1453 (2018).
- DePaolo, D. J. Isotopic effects in fracture-dominated reactive fluid-rock systems. Geochim. Cosmochim. Acta 70, 1077-1096 (2006).
- Norton, D. & Taylor, H. Jr Quantitative simulation of the hydrothermal systems of crystallizing magmas on the basis of transport theory and oxygen isotope data: an analysis of the Skaergaard intrusion. *J. Petrol.* 20, 421–486 (1979).
- Wunsch, C. The Ocean Circulation Inverse Problem (Cambridge Univ. Press, 1996).
- Wing, B. A. & Ferry, J. M. Three-dimensional geometry of metamorphic fluid flow during Barrovian regional metamorphism from an inversion of combined petrologic and stable isotopic data. *Geology* 30, 639–642 (2002).
- Wing, B. A. & Ferry, J. M. Magnitude and geometry of reactive fluid flow from direct inversion of spatial patterns of geochemical alteration. *Am. J. Sci.* 307, 793–832 (2007).
- 22. Taylor, H. P. Water/rock interactions and the origin of $\rm H_2O$ in granitic batholiths: thirtieth William Smith lecture. *J. Geolog. Soc.* 133, 509–558 (1977).

Cathles, L. M. in *The Kuroko and Related Volcanogenic Massive Sulfide Deposits* Vol. 5 (eds Ohmoto, H. & Skinner, B. J.) 439–487 (Economic Geology Publishing, 1983).

- Taylor, H. P. Jr & Forester, R. W. An oxygen and hydrogen isotope study of the Skaergaard intrusion and its country rocks: a description of a 55-M.Y. old fossil hydrothermal system. J. Petrol. 20, 355-419 (1979).
- Gillis, K. M., Muehlenbachs, K., Stewart, M., Gleeson, T. & Karson, J. Fluid flow patterns in fast spreading East Pacific Rise crust exposed at Hess Deep. J. Geophys. Res. Solid Earth 106, 26311–26329 (2001).
- Green, G. R., Ohmoto, H., Date, J. & Takahashi, T. in *The Kuroko and Related Volcanogenic Massive Sulfide Deposits* Vol. 5 (eds Ohmoto, H. & Skinner, B. J.) 395–411 (Economic Geology Publishing, 1983).
- Schiffman, P. & Smith, B. M. Petrology and oxygen isotope geochemistry of a fossil seawater hydrothermal system within the Solea graben, northern Troodos ophiolite, Cyprus. J. Geophys. Res. Solid Earth 93, 4612–4624 (1988).
- Mukasa, S. B. & Ludden, J. N. Uranium-lead isotopic ages of plagiogranites from the Troodos ophiolite, Cyprus, and their tectonic significance. *Geology* 15, 825–828 (1987).
- Lear, C., Elderfield, H. & Wilson, P. Cenozoic deep-sea temperatures and global ice volumes from Mg/Ca in benthic foraminiferal calcite. *Science* 287, 269–272 (2000).
- 30. Vearncombe, S. et al. 3.26 Ga black smoker-type mineralization in the Strelley Belt, Pilbara Craton, Western Australia. *J. Geol. Soc.* **152**, 587–590 (1995).
- Brauhart, C. W., Groves, D. I. & Morant, P. Regional alteration systems associated with volcanogenic massive sulfide mineralization at Panorama, Pilbara, Western Australia. *Econ. Geol.* 93, 292–302 (1998).
- 32. Buick, R. et al. Geochronology and stratigraphic relationships of the Sulphur Springs Group and Strelley Granite: a temporally distinct igneous province in the Archaean Pilbara Craton, Australia. *Precambrian Res.* 114, 87–120 (2002).
- Van Kranendonk, M. J. et al. Making it thick: a volcanic plateau origin of Palaeoarchean continental lithosphere of the Pilbara and Kaapvaal cratons. Geol. Soc. Spec. Publ. 389, 83–111 (2015).
- 34. Kato, Y. & Nakamura, K. Origin and global tectonic significance of Early Archean cherts from the Marble Bar greenstone belt, Pilbara Craton, Western Australia. *Precambrian Res.* 125, 191–243 (2003).
- Nijman, W., Kloppenburg, A. & de Vries, S. T. Archaean basin margin geology and crustal evolution: an East Pilbara traverse. J. Geol. Soc. 174, 1090–1112 (2017).
- Martindale, J., Hagemann, S., Huston, D. & Danyushevsky, L. Integrated stratigraphic-structural-hydrothermal alteration and mineralisation model for the Kangaroo Caves zinc-copper deposit, Western Australia. *Aust. J. Earth* Sci. 61, 159–185 (2014).
- Huston, D. L., Brauhart, C. W., Drieberg, S. L., Davidson, G. J. & Groves, D. I. Metal leaching and inorganic sulfate reduction in volcanic-hosted massive sulfide mineral systems: evidence from the paleo-Archean Panorama district Western Australia. *Geology* 29, 687–690 (2001).
- Brauhart, C. W., Huston, D. L., Groves, D. I., Mikucki, E. J. & Gardoll, S. J. Geochemical mass-transfer patterns as indicators of the architecture of a complete volcanic-hosted massive sulfide hydrothermal alteration system, Panorama District, Pilbara, Western Australia. *Econ. Geol.* 96, 1263–1278 (2001).
- Drieberg, S. L. et al. The interplay of evolved seawater and magmatichydrothermal fluids in the 3.24 Ga Panorama volcanic-hosted massive sulfide hydrothermal system, North Pilbara Craton, Western Australia. *Econ. Geol.* 108, 79–110 (2013).
- Brauhart, C., Huston, D. & Andrew, A. Oxygen isotope mapping in the Panorama VMS district, Pilbara Craton, Western Australia: applications to estimating temperatures of alteration and to exploration. *Mineral. Depos.* 35, 727–740 (2000).
- Pope, E. C., Bird, D. K. & Rosing, M. T. Isotope composition and volume of Earth's early oceans. *Proc. Natl Acad. Sci. USA* 109, 4371–4376 (2012).
- Silverman, S. R. The isotope geology of oxygen. Geochim. Cosmochim. Acta 2, 26–42 (1951).
- Gregory, R. T. in Stable Isotope Geochemistry: A tribute to Samuel Epstein Vol. 3 (eds Taylor, Jr., H. P., O'Neil, J. R. & Kaplan, I. R.) 65–76 (Geochemical Society, 1991).
- Eiler, J. M. Oxygen isotope variations of basaltic lavas and upper mantle rocks. Rev. Mineral. Geochem. 43, 319–364 (2001).
- Lebrun, T. et al. Thermal evolution of an early magma ocean in interaction with the atmosphere. J. Geophys. Res. Planets 118, 1155–1176 (2013).
- Holland, H. D. The Chemical Evolution of the Atmosphere and Oceans (Princeton Univ. Press, 1984).
- Korenaga, J. Initiation and evolution of plate tectonics on Earth: theories and observations. Annu. Rev. Earth Planet. Sci. 41, 117–151 (2013).
- 48. Buick, R. et al. Record of emergent continental crust ~3.5 billion years ago in the Pilbara craton of Australia. *Nature* **375**, 574–577 (1995).
- Grandstaff, D., Edelman, M., Foster, R., Zbinden, E. & Kimberley, M. Chemistry and mineralogy of Precambrian paleosols at the base of the

- Dominion and Pongola Groups (Transvaal, South Africa). *Precambrian Res.* **32**, 97–131 (1986).
- 50. Bindeman, I., Bekker, A. & Zakharov, D. Oxygen isotope perspective on crustal evolution on early Earth: a record of Precambrian shales with emphasis on paleoproterozoic glaciations and great oxygenation event. *Earth Planet. Sci. Lett.* 437, 101–113 (2016).
- 51. Korenaga, J., Planavsky, N. J. & Evans, D. A. Global water cycle and the coevolution of the Earth as interior and surface environment. *Phil. Trans. R. Soc. A* 375, 20150393 (2017).
- 52. Taylor, S. R. & McLennan, S. M. The geochemical evolution of the continental crust. *Rev. Geophys.* 33, 241–265 (1995).
- 53. Simon, L. & Lècuyer, C. Continental recycling: the oxygen isotope point of view. *Geochem. Geophys. Geosyst.* **6**, Q08004 (2005).
- Molnar, P. Gravitational potential energy per unit area as a constraint on Archean sea level. Geochem. Geophys. Geosyst. 19, 4063–4095 (2018).
- Cowan, N. B. & Abbot, D. S. Water cycling between ocean and mantle: super-earths need not be waterworlds. Astrophys. J. 781, 27 (2014).

Publisher's note Springer Nature remains neutral with regard to jurisdictional claims in published maps and institutional affiliations.

© The Author(s), under exclusive licence to Springer Nature Limited 2020

Table 1 Results of sensitivity analysis accounting for a hydrated mineral sink								
Setting	$\delta R_{\rm i}$	F/R	Hydrated F/R	Hydrated δ ¹⁸ O	Inverse δ¹8O	Difference		
East Pacific Rise	5.5	0.45 ± 0.01	0.008	0.21	0.23	0.02		
Fukazawa	7.5	3.04 ± 0.26	0.097	-0.46	-0.51	-0.05		
Solea	5.5	1.25 ± 0.08	0.044	-1.07	-1.08	-0.01		
Panorama	5.5	0.87 ± 0.04	0.048	3.31	3.27	-0.04		

Methods

From natural samples or forward model output, we build a regularly spaced, contoured grid of both oxygen isotope and temperature data. For natural outcrops, we correct the spatially located raw data for tilting, faulting and/or folding. Once the data are projected onto a common vertical plane, we interpolate onto a regularly spaced grid to make a common basis for oxygen isotope and temperature fields (Fig. 1).

For each grid box, we assume that the altering fluid is water, and that the amount of fluid that enters equals the amount of fluid that leaves (that is, fluid mass balance). This assumption is equivalent to the requirement that the total amount of oxygen in the rocks in each box remains the same. We also assume that the difference in the amount of ¹⁸O that is carried into and out of each grid box by the fluid is equal to the ¹⁸O that is taken up or released by the rock in that box through isotopic exchange reactions (that is, isotope mass balance).

For all grid boxes, we apply the following mass-balance matrix equation:

$$N = Cq \tag{1}$$

where, for each local grid box, **N** represents the change in ^{18}O in the rock from an assigned initial value to the final measured value, **C** is the ^{18}O concentration in the fluid after exchange with the rock and **q** is the time-integrated amount of fluid (in moles) that passed through the local rock volume. Note that we transform measured $\delta^{18}O$ values to ratios of $^{18}O/^{18}O$. Since $^{16}O\approx$ total oxygen (8.6 × 106 mol oxygen per cubic metre of rock. We multiply **N** by the total number of moles of oxygen in each grid cell to calculate the total ^{18}O gained or lost. Assigned starting rock $\delta^{18}O$ values are 5.5% for most oceanic crustal sections except the synthetic data from ref. 21 , for which re-examination of original model code indicates an initial $\delta^{18}O=5.7\%$, and Fukazawa, which had an initial $\delta^{18}O=7.5\%$ (ref. 20). We assumed a starting $\delta^{18}O$ of 7% for plagioclase in Skaergaard rocks. At each grid cell boundary, we assumed that equilibrium isotopic exchange between the rock and the fluid, where the difference in $\delta^{18}O$ between rock and fluid is Δ_{R-19} was a function of temperature (T) alone:

$$\Delta_{R-F} = -3.9 \times 10^3 / T + 3.43 \times 10^6 / T^2$$
 (2)

from ref. $^{\rm 57}$. Temperature estimates are independent from oxygen isotope values or are imposed. All temperatures are in Kelvin. For natural settings, we calculate the isotopic value of a fluid in equilibrium with rock based on the final measured $\delta^{\rm 18}O$ value of the rock.

Critically, the inverse technique enforces oxygen and fluid mass balance both at local and system-wide scales. We assumed that there was no production or consumption of water during hydrothermal alteration. In addition, this implies that the amount of fluid that enters each grid box is equal to the amount of fluid that exits each grid box. We imposed no fluid flow along the bottom of the entire inversion domain but the top and sides were open to fluid flow.

We also added a smoothing parameter, α^2 , which weights solutions towards those where fluid flow through neighbouring grid boxes matches more closely. Specifically, to solve for $\tilde{\mathbf{q}}$, where the tilde indicates this is an approximation of the true value of \mathbf{q} , we applied the following matrix calculation:

$$\tilde{\mathbf{q}} = (\mathbf{C}^{\mathrm{T}}\mathbf{C} + \boldsymbol{\alpha}^{2}\mathbf{I})^{-1}\mathbf{C}^{\mathrm{T}}\mathbf{N}$$
 (3)

where C^T is the transpose of the concentration matrix, I is an identity matrix and α^2 is the smoothing parameter, which was constrained to be 2.05×10^{-4} via inversion of the forward model results from ref. 21 under the constraint of an input fluid of $\delta^{18}O = 0\%$.

We solved this equation to estimate the total moles of fluid oxygen (F), which is the norm of the vector $\tilde{\mathbf{q}}$, that circulated through a given package of rock characterized by a fixed total number of moles of rock oxygen (R). To estimate uncertainty in F, we ran the inversion n times for each geologic setting, where n is the total number of samples, and each time removed a random data point (Supplementary Table 2).

We then calculated whole-system fluid/rock (F/R) ratios. This is related to the average δ^{18} O value of seawater that infiltrated the hydrothermal system over the lifetime of alteration (δW_i) through:

$$\delta W_i = \frac{\delta R_f - \delta R_i}{F/R} + \delta R_f - \Delta_{R-F} \tag{4}$$

where δR_r is the final average rock δ^{18} O, which is measured, and Δ_{R-F} is the average difference between the δ^{18} O of fluid and rock in the system²². We calculated an

average temperature of alteration, and therefore $\Delta_{\text{R-P}}$ for each inversion area (Supplementary Table 2).

We acknowledge that hydration of rock and formation of hydrated minerals means that strict mass balance between fluxes across each grid box may not be true in natural systems. This effect, however, is minor compared to the total amount of fluid that alters a certain rock volume. We quantify this effect using the following, empirical relationship from ref. ¹¹ that relates altered basalt water weight percent $(\beta=0.97\%c/wt\%)$ to final rock $\delta^{18}O$ (δR_c):

$$\delta R_f = \beta + \delta R_i \tag{5}$$

and its initial δ^{18} O (δR_i). We calculated an estimated water content using the δR_f from each of the natural sample site grids (Extended Data Fig. 3). We converted weight percent water to total moles of oxygen in hydrated minerals, then calculated a corresponding fluid/rock ratio solely due to hydration (Table 1). We subtracted this value from the one returned in the inversion, since hydration represents an oxygen sink into minerals.

Then we used equation (4), with this corrected, 'hydrated' fluid/rock ratio to calculate an estimated initial fluid $\delta^{18}O$ (δW_i^h). We find the difference between δW_i from the inversion and δW_i^h using the hydrated fluid/rock ratio to be no greater than 0.1% (Table 1). Thus, we neglect the minor influence of hydrated minerals in the inversion, and assume negligible hydration fluid sinks in overall fluid mass balance.

The choice of initial rock $\delta^{18}O$ affects the estimated $\delta^{18}O$ of incoming fluid. Specifically for Panorama, if the entire volcanic package had the same $\delta^{18}O$ as unaltered Strelley Granite (7.9%), rather than 5.5%, then the inversion returns an estimate for incoming seawater of $0.03\pm0.09\%$. We suggest, however, that initial rock $\delta^{18}O$ values were likely to be near 5.5% at Panorama. First, the $\delta^{18}O$ value of the mantle, and mantle-derived ocean crust, is thought to be constant over Earth history (for example, ref. ¹). Second, the small ^{18}O enrichment seen in the Strelley Granite is a common feature in felsic rocks, such as plagiogranites, associated with mantle-derived basalts and gabbros from mid-ocean ridge environments and ophiolites $^{38-60}$. Although assimilation of ^{18}O -enriched wall rocks can also elevate $\delta^{18}O$ values in silicic magmas, potentially negating any genetic reasons for the isotopic similarity between the Strelley Granite and evolved rocks such as plagiogranites, detailed mapping of contact relationships suggests that the Strelley Granite intruded in a sill-like manner 31 , and is thus unlikely to have assimilated much of the local volcanic pile.

Data availability

Oxygen isotope data and associated spatial data were previously published in refs. ^{18,21,23,25,26,40}. Temperature data are mostly from the same references as the oxygen isotope data, with the exception of those for Panorama, which were from ref. ³⁹.

We have provided all data used in the inversions in csv files in the Supplementary Information.

Code availability

All model code and data used for inversions are available in the Supplementary Information and on the corresponding author's github repository (https://github.com/benwjohnson). In addition, the corresponding author is happy to send code upon email request.

References

- Laverne, C., Agrinier, P., Hermitte, D. & Bohn, M. Chemical fluxes during hydrothermal alteration of a 1200-m long section of dikes in the oceanic crust, DSDP/ODP Hole 504B. Chem. Geol. 181, 73–98 (2001).
- Cole, D. R., Mottl, M. J. & Ohmoto, H. Isotopic exchange in mineral-fluid systems. II. Oxygen and hydrogen isotopic investigation of the experimental basalt-seawater system. *Geochim. Cosmochim. Acta* 51, 1523–1538 (1987).
- Stakes, D. S. & Taylor, H. P. in *Ophiolites in Earth History* Vol. 218 (eds Dilek, Y. & Robinson, P. T.) 315–351 (Geological Society, 2003).
- Wanless, V. et al. Volatile abundances and oxygen isotopes in basaltic to dacitic lavas on mid-ocean ridges: the role of assimilation at spreading centers. Chem. Geol. 287, 54–65 (2011).
- Grimes, C. B., Ushikubo, T., Kozdon, R. & Valley, J. W. Perspectives on the origin of plagiogranite in ophiolites from oxygen isotopes in zircon. *Lithos* 179, 48–66 (2013).

Acknowledgements

We acknowledge NSF grant support for B.W.J. (EAR-PF 1725784) and B.A.W. (EF 1724393), as well as the American Philosophical Society's Lewis and Clark Grant for field work in Astrobiology to B.W.J. We thank C. Brauhart for discussions on the geology of Panorama and guidance in the field, and E. Pope for constructive criticism that materially improved the paper in scope and detail.

Author contributions

B.W.J. and B.A.W. conceived the project. B.A.W. developed the inverse method. B.W.J. performed the data assimilation, inverse modelling and ocean isotope exchange modelling. B.W.J. and B.A.W. interpreted model results and wrote the manuscript.

Competing interests

The authors declare no competing interests.

Additional information

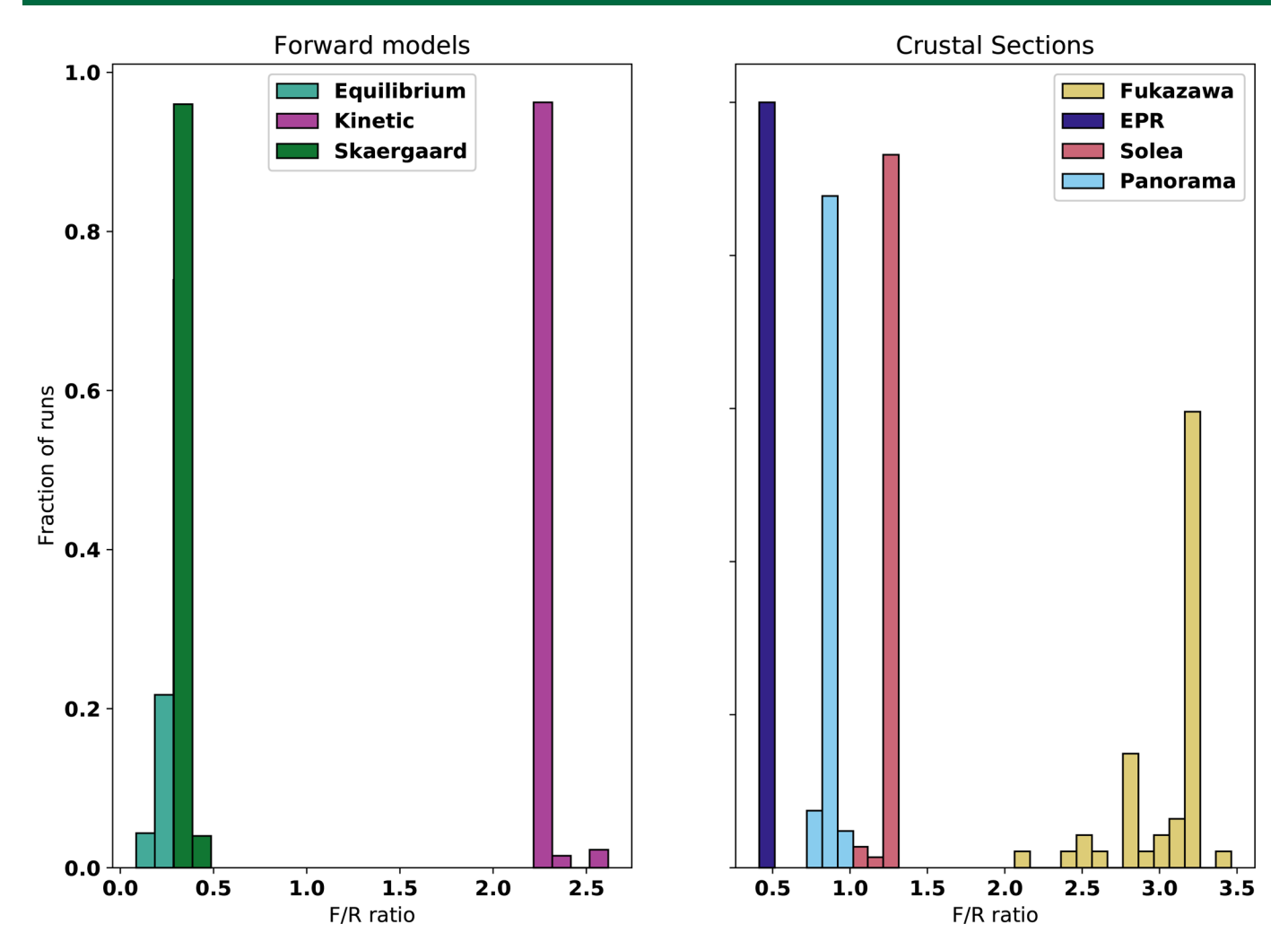
Extended data is available for this paper at https://doi.org/10.1038/s41561-020-0538-9.

Supplementary information is available for this paper at https://doi.org/10.1038/s41561-020-0538-9.

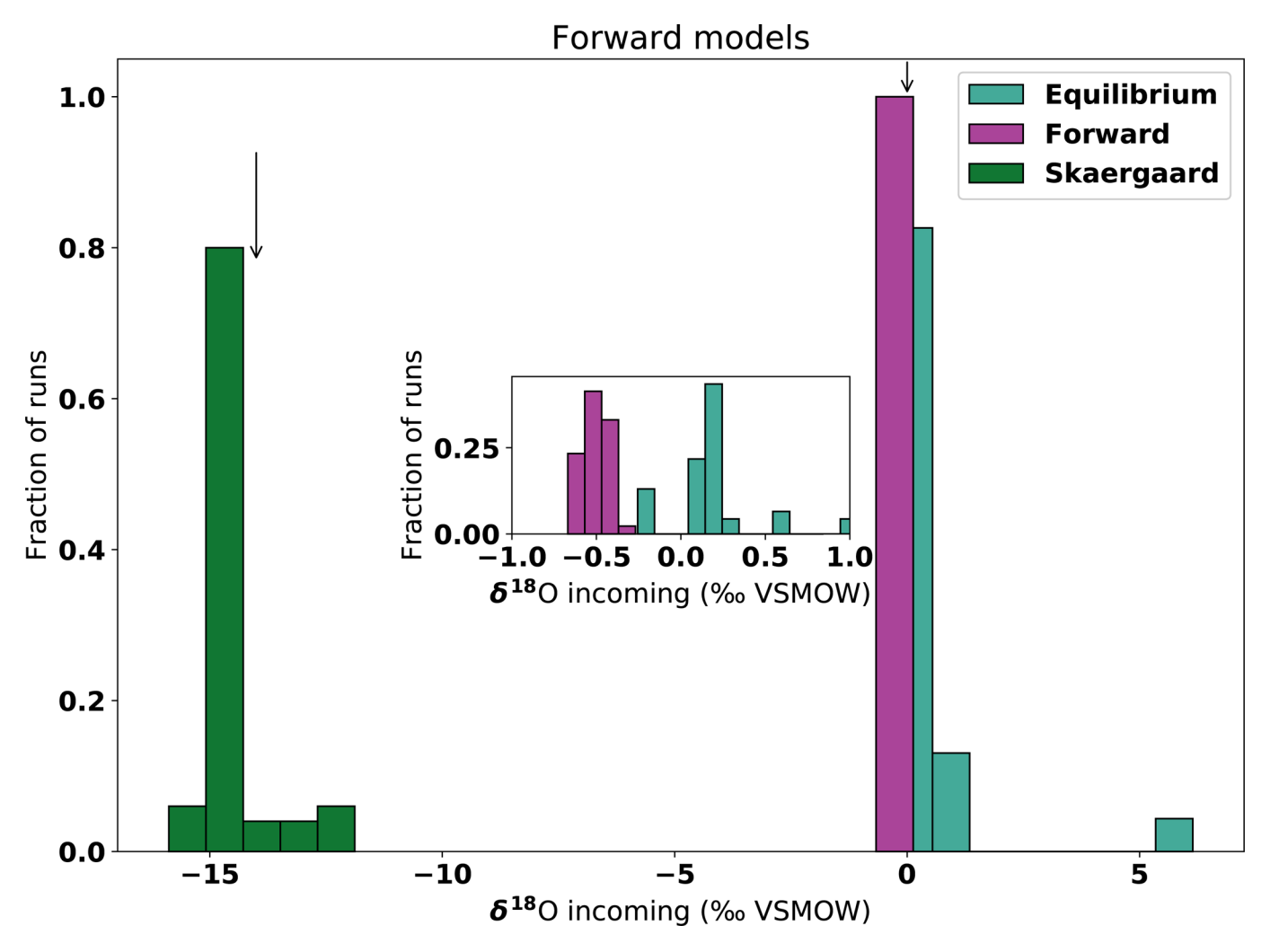
Correspondence and requests for materials should be addressed to B.W.J.

Peer review information Primary Handling Editor: Rebecca Neely.

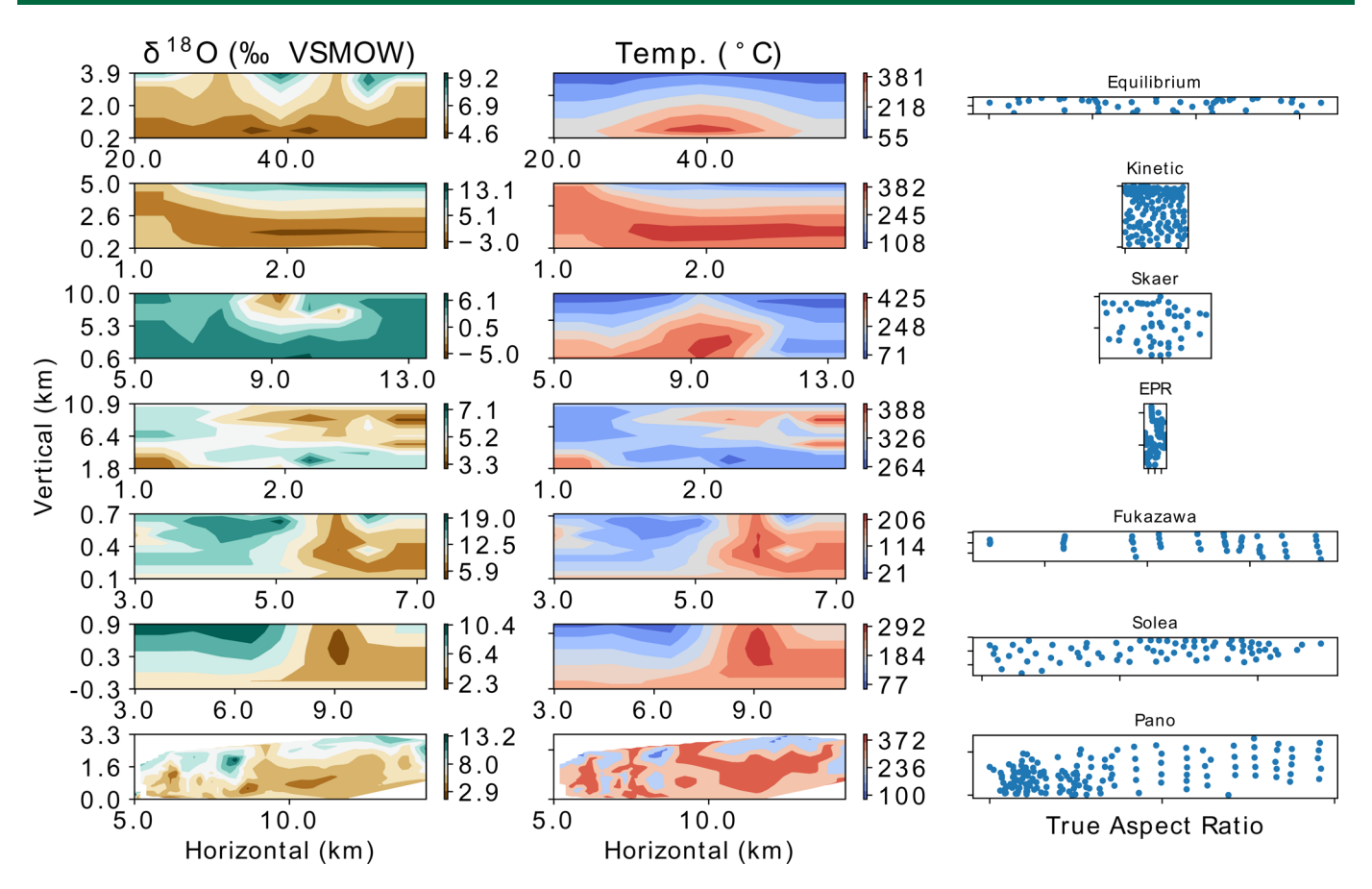
Reprints and permissions information is available at www.nature.com/reprints.



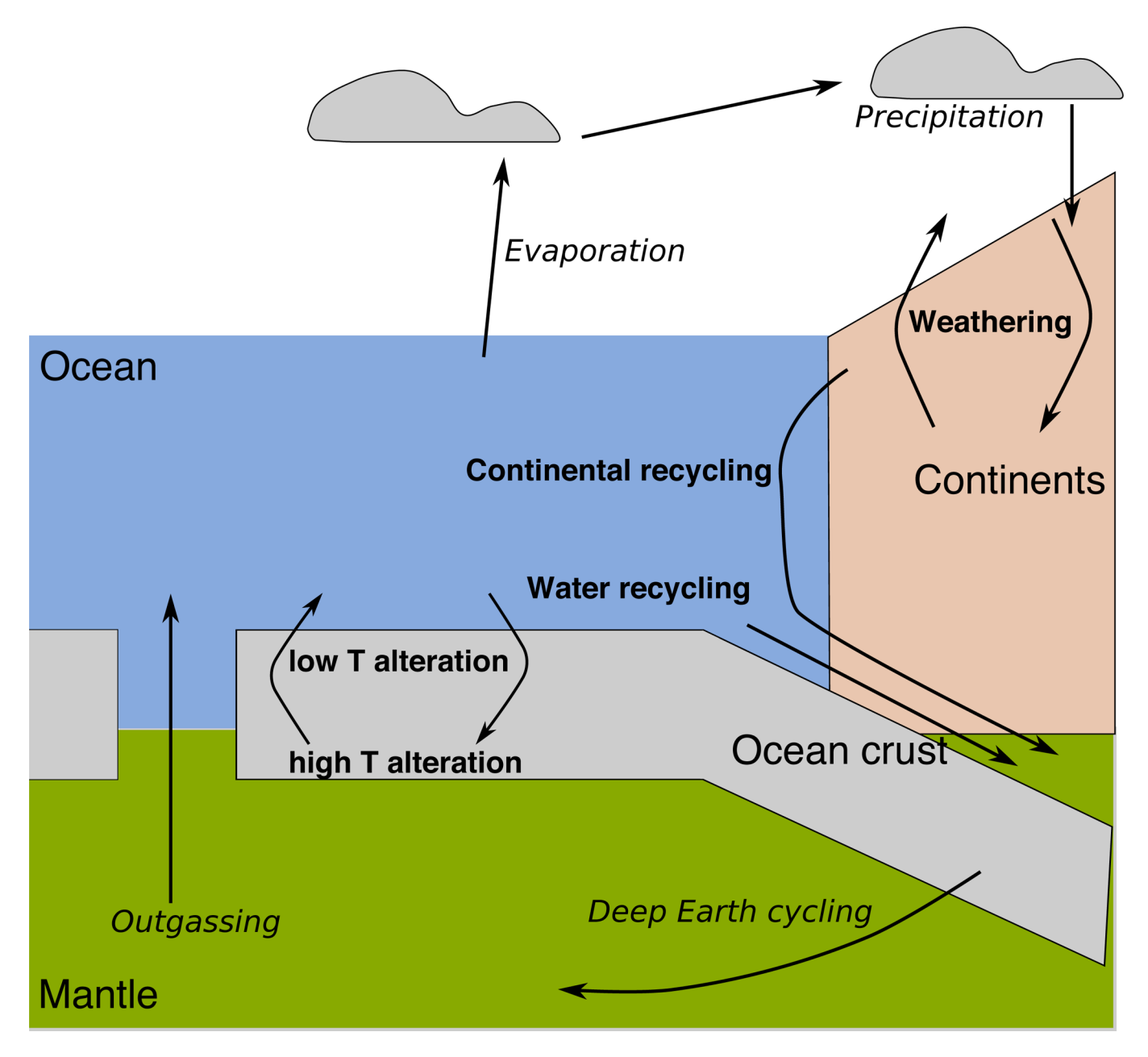
Extended Data Fig. 1 | Estimated fluid rock ratios for 'leave-one-out' inversions. Water/rock ratio results of 'leave-one-out' inversions, removing one sample each time for all synthetic datasets (21; 18; 23).



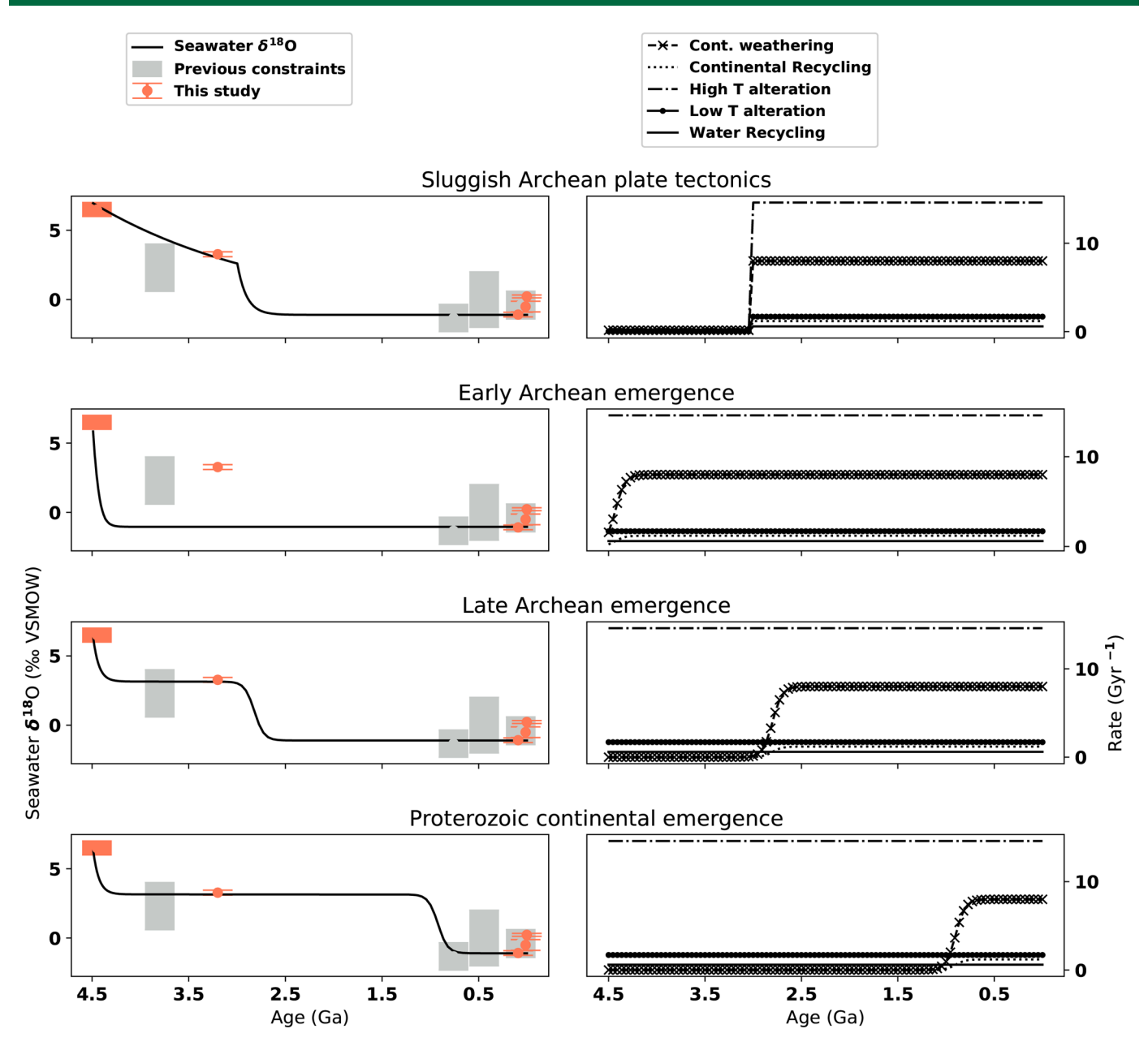
Extended Data Fig. 2 | **Estimated incoming fluid oxygen isotope composition from synthetic datasets.** Results of 'leave-one-out' inversions, removing one sample each time (21; 18; 23). Each set of inversions has the same number of runs as there are samples for each set. Arrows indicate imposed incoming fluid δ^{18} O, and inset shows the models on the same isotopic scale as the crustal sections in Fig. 2.



Extended Data Fig. 3 | δ¹⁸O and temperature contours for all datasets. The third column shows the true aspect ratio of all datasets, highlighting that the geometry of the study area does not affect inverse estimates.



Extended Data Fig. 4 | Schematic of the Earth system water cycle. Fluxes in bold are used in the kinetic model for seawater δ^{18} O, while those in italics are not considered to be important isotopically for the long-term evolution of seawater δ^{18} O.



Extended Data Fig. 5 | Modeled oxygen isotope exchange rates over time. Oxygen isotope exchange rates used to make different δ^{18} O curves in Figure 3. We assume 2 - 4% modern exchange rates initially for the first row, which then increase to modern rates by 2.5 Ga The second through fourth rows impose continental emergence at 4.4, 3, and 0.9 Ga, increasing to modern values over \approx 500 million years.



SUPPLEMENTARY INFORMATION

https://doi.org/10.1038/s41561-020-0538-9

In the format provided by the authors and unedited.

Limited Archaean continental emergence reflected in an early Archaean ¹⁸O-enriched ocean

Benjamin W. Johnson ^{1,2} and Boswell A. Wing¹

¹Department of Geological Sciences, University of Colorado Boulder, Boulder, CO, USA. ²Department of Geological and Atmospheric Sciences, Iowa State University, Ames, IA, USA. [™]e-mail: bwj@iastate.edu

Limited Archean continental emergence reflected in an early Archean ¹⁸O-enriched ocean Supplemental Information

Benjamin W Johnson,^{1,2*} Boswell A Wing¹

¹Department of Geological Sciences, University of Colorado Boulder,
2200 Colorado Avenue, Boulder, CO, USA, 80309
²Department of Geological and Atmospheric Sciences, Iowa State University,
253 Science Hall, 2237 Osborn Drive, Ames, IA, USA, 50011

*To whom correspondence should be addressed; E-mail: bwj@iastate.edu.

Supplemental Information

Forward model output inversion results

As described in the main text, we tuned the smoothing parameter in our model using forward model output from (1), and further tested the inverse method on synthetic data from (2) and (3). The results are shown in Fig. S1. The subplot shows the results on the same scale as results from natural datasets. In addition, we show isotope and temperature contour plots in Figure S3.

Kinetic modeling of seawater δ^{18} O

Using the approach of (4), we calculate steady-state seawater $\delta^{18}{\rm O}$ values with:

$$\delta W_{\text{steady-state}} \equiv \left[\sum k_i (\delta_i^o - \Delta_i) \right] / \sum k_i$$
 (Eq. S1)

where the k_i are rate constants normalized to modern ocean mass, the δ_i^o are starting rock δ^{18} O values, and the Δ_i are the bulk O-isotope fractionation factor between different rock reservoirs (i) and water (Table S1). Important O-isotope exchange fluxes on geological timescales are shown in Figure S4 and include: high-temperature and low-temperature alteration of oceanic crust, continental weathering, and recycling of continentally-derived water in subduction zones.

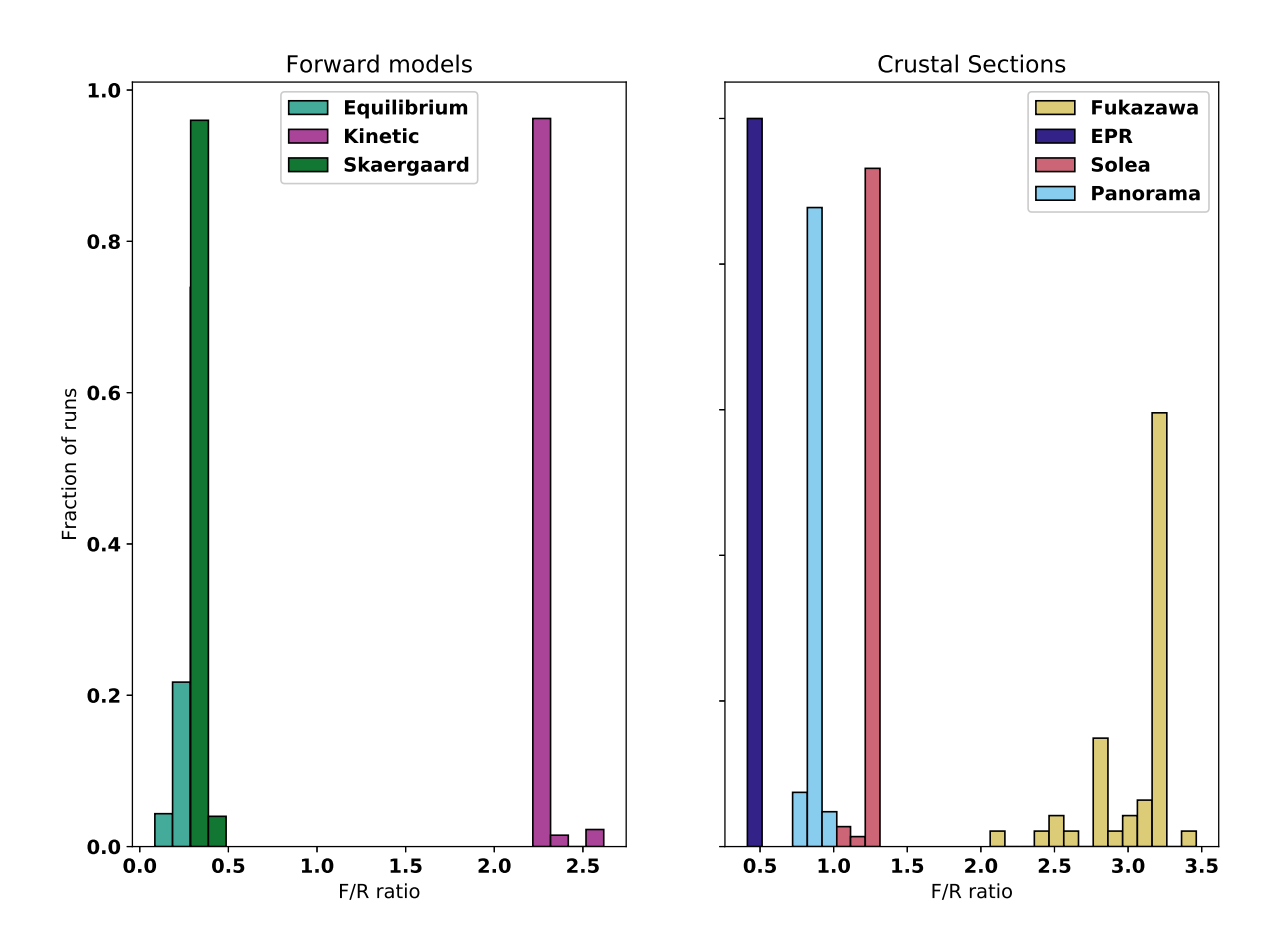


Figure S1: Water/rock ratio results of 'leave-one-out' inversions, removing one sample each time for all synthetic datasets (1; 3; 2).

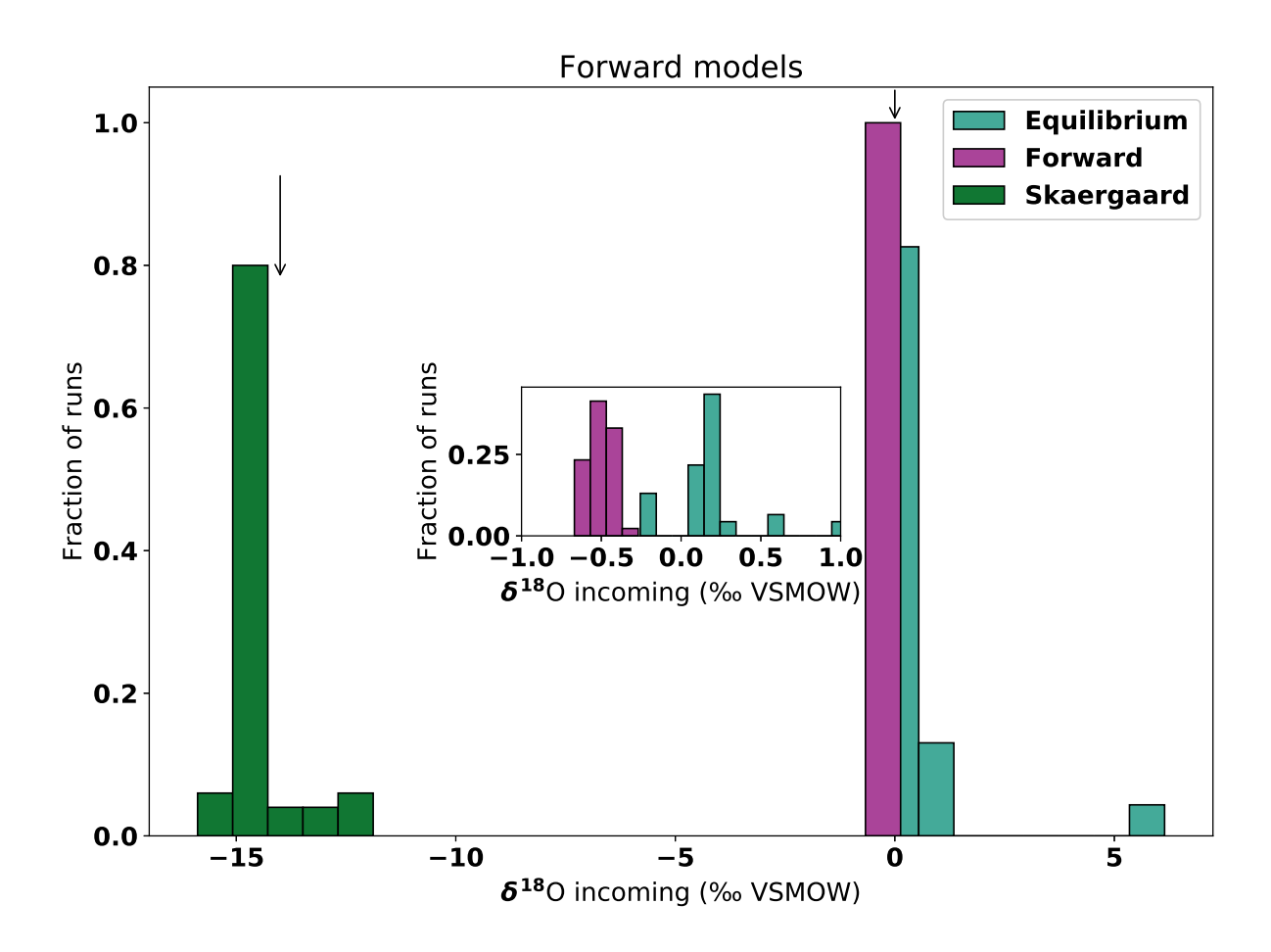


Figure S2: Results of 'leave-one-out' inversions, removing one sample each time for all synthetic (1; 3; 2). Each set of inversions has the same number of runs as there are samples for each set. Arrows indicate imposed incoming fluid δ^{18} O, and inset shows the Wing & Ferry and Cathles models on the same isotopic scale as the crustal sections in Fig. 2.

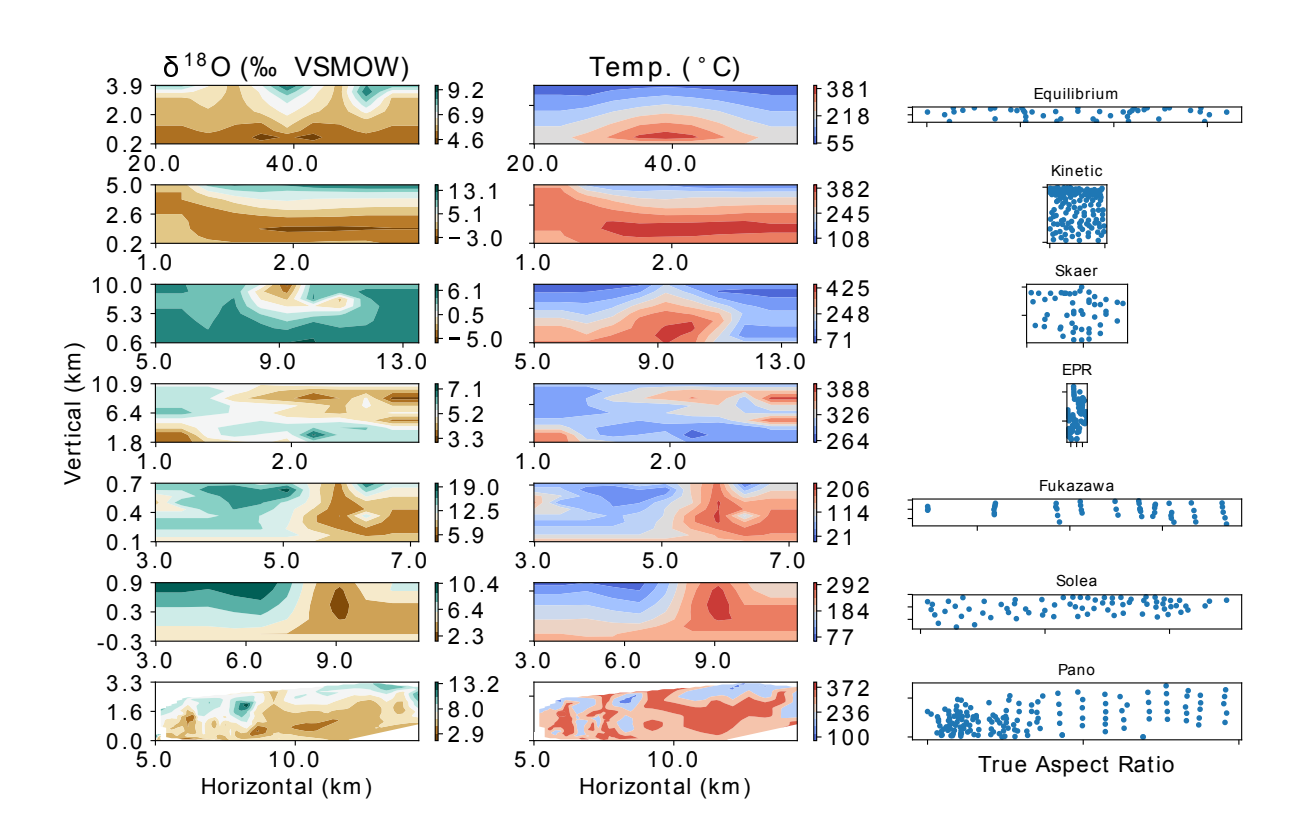


Figure S3: δ^{18} O and temperature contours for all datasets, with oxygen isotope in %. The third column shows the true aspect ratio of all datasets, highlighting that the geometry of the study area does not affect inverse estimates.

Table S1: Values used in Equations Eq. S1 -Eq. S2 to calculate seawater $\delta^{18}O$ over time. All values except Δ for continental weathering and Archean high temperature alteration are from (5). We adjusted continental weathering to reproduce a -1% modern ocean, and adjusted high temperature alteration to shift from 1.4 to 4.1% for the middle continental emergence scenario. All other scenarios use 4.1% for this fractionation factor. All k_i values are normalized to the current ocean mass and represent the amount of time it takes to process a modern ocean's-worth of O in a billion years.

Flux	k_i (Gyr ⁻¹)	Δ (‰)	δ^o (‰)
Continental Weathering	8.0	13	7.8
Continental Recycling	1.2	9.8	7.8
High Temperature alteration	14.6	1.6 - 4.2	5.5
Low Temperature Alteration	1.7	9.3	5.5
Water Recycling	0.6	2.5	7.0

Then, we apply the equation for the dynamic δ^{18} O of seawater, assuming at each time point k_i , δ^o_i , and Δ_i are held constant and starting ocean δ^{18} O (δW_o) is 7‰:

$$\delta W = (\delta W_o - \delta W_{\text{steady-state}})e^{-\Sigma k_i t} + \delta W_{\text{steady-state}}$$
 (Eq. S2)

The continental fluxes are "turned on" at 3 Ga, consistent with initial continental emergence at this time (Fig. S5), and reach modern values by 2.5 Ga. We also present similar calculations for early emergence a 4.4 Ga, and late emergence at 0.9 Ga. Our results are inconsistent with early emergence, but testing for later emergence requires additional inverse analysis of Proterozoic altered oceanic crust.

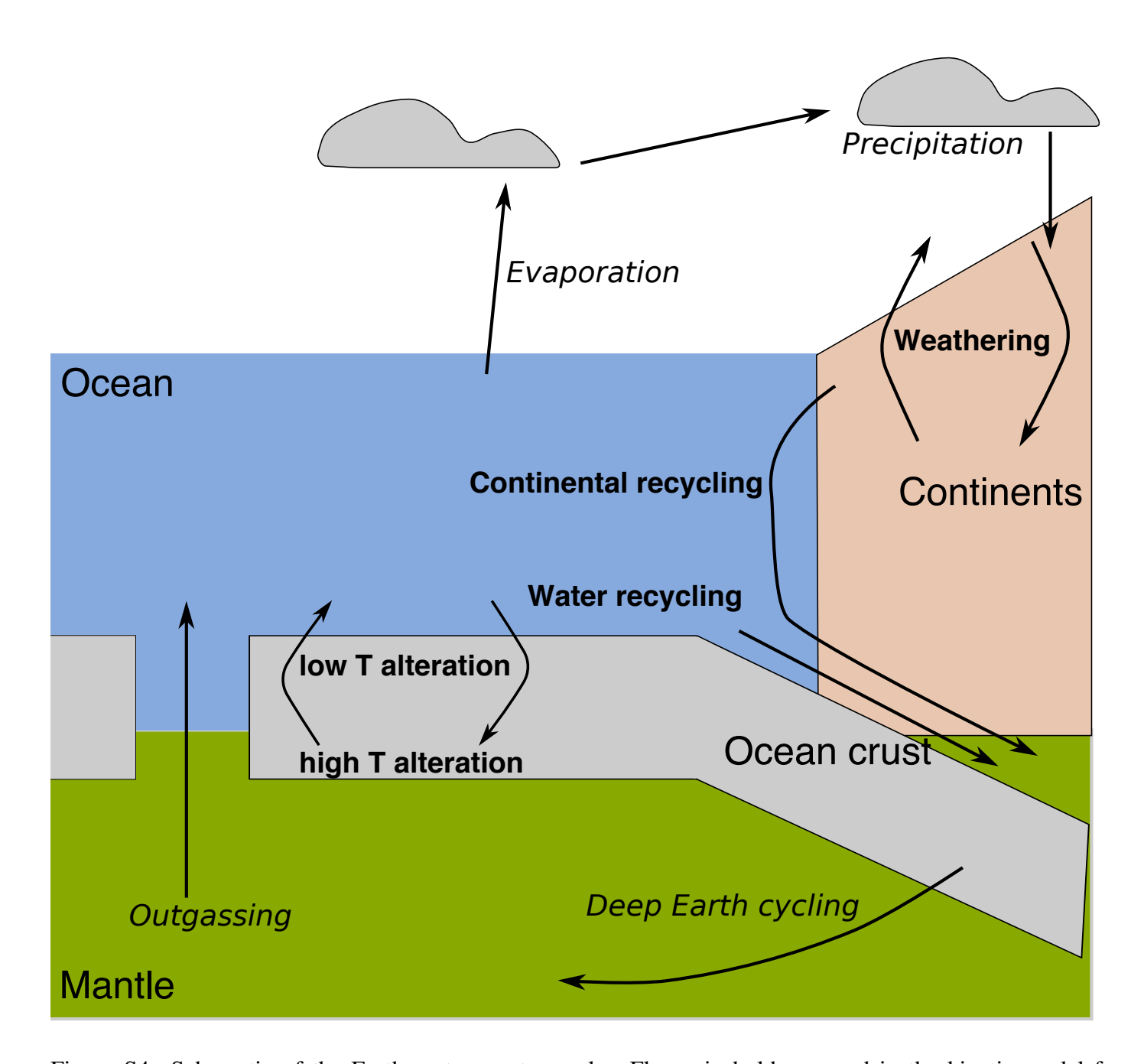


Figure S4: Schematic of the Earth system water cycle. Fluxes in bold are used in the kinetic model for seawater δ^{18} O, while those in italics are not considered to be important isotopically for the long-term evolution of seawater δ^{18} O.

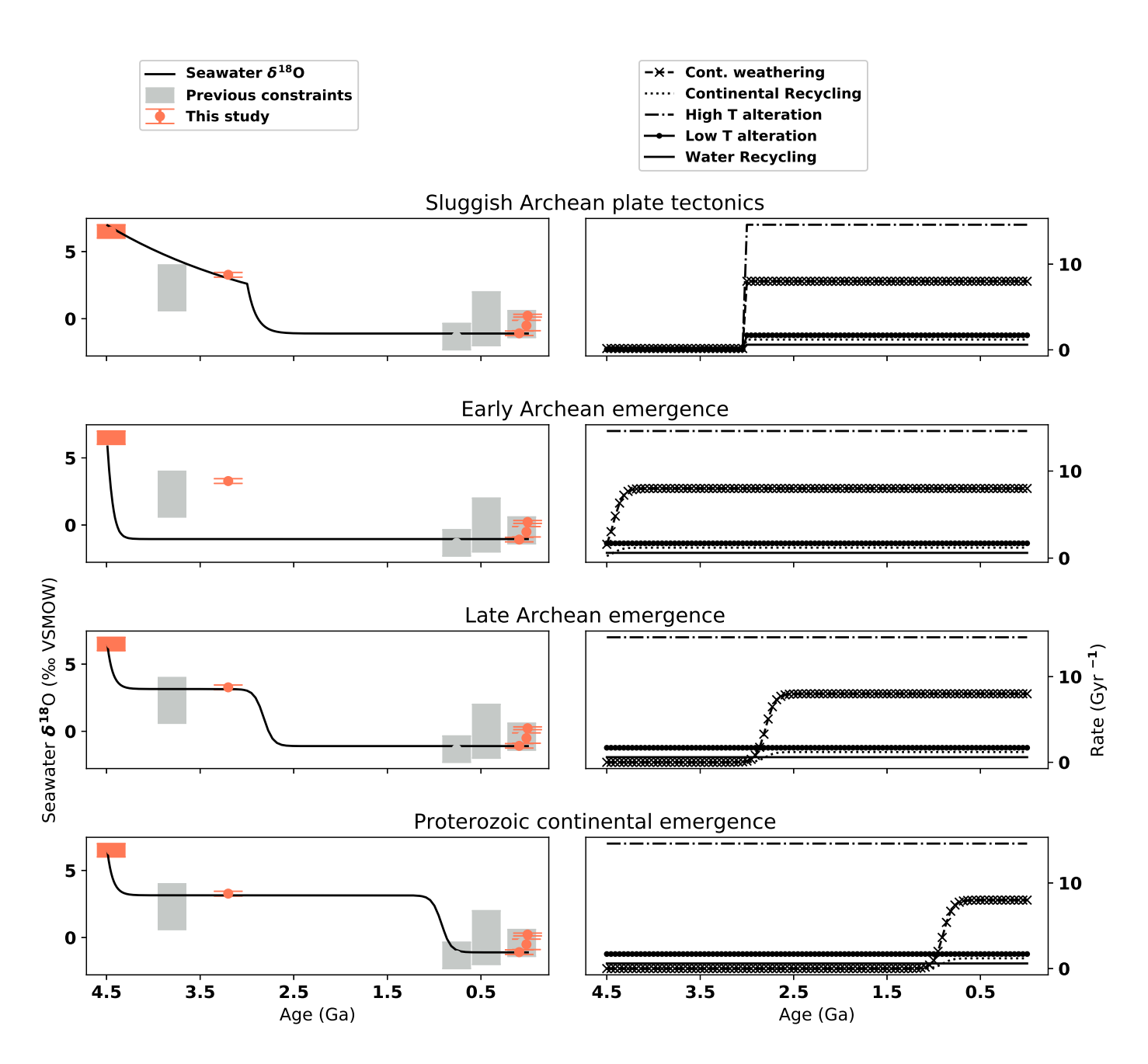


Figure S5: Oxygen isotope exchange rates used to make different δ^{18} O curves in Figure 3. We assume 2-4% modern exchange rates initially for the first row, which then increase to modern rates by 2.5 Ga The second through fourth rows impose continental emergence at 4.4, 3, and 0.9 Ga, increasing to modern values over \approx 500 million years

•

Table S2: Conditions for and results of inversion of forward model output and natural samples. n is the number of samples from each, and temperature is the average temperature of alteration over the entire regularly spaced grid. Incoming δ^{18} O column is either forward model input or (δR_f) rock values are given, along with average fractionation between rock and fluid (Δ) . δ^{18} O and Δ are in %, and all inversion estimates show known Mesozoic-Cenozoic seawater compositions. Note we do not include one outlier from (1) in the mean calculation. Starting (δR_i) and final mean δ^{18} O values with two standard deviations

	Rock F/R Δ δR_i δR_f	0.28 ± 0.05 8.46 5.7	2.25 ± 0.04 3.98 7.5	0.33 ± 0.02 7.44 7.0	0.45 ± 0.01	3.04 ± 0.26 13.45 7.5	1.25 ± 0.08 7.70 5.5	0.87 ± 0.04 5.69 5.5	
	Moles O Rock	$2.3 \pm 0.06 \times 10^{13}$	$1.6 \pm 0.0 \times 10^{12}$	1.0 ± 0.01	$2.1 \pm 0.01 \times 10^{12}$	$3.9 \pm 0.0 \times 10^{11}$	1.0 ± 0.0	$4.9 \pm 0.07 \times 10^{12}$	
	Moles O Fluid							$8.5 \pm 0.38 \times 10^{12}$	
	Inverse δ^{18} O	0.19 ± 0.29	-0.52 ± 0.08	-14.39 ± 0.74	0.23 ± 0.05	-0.51 ± 0.19	-1.08 ± 0.08	3.27 ± 0.09	
	Temp (°C) Incoming δ^{18} O	0	0	-14	0.2	-0.55	-1	ı	
	Temp (°C)	160	251	235	322	121	191	254	
	u	46	133	50	85	47	73	188	// 0 /1/
mean o - O values v	Setting ^{ref} n Temp (°C) Incomi	$oxed{ ext{Equilibrium}^1}$	Kinetic ²	$Skeargaard^3$	East Pacific Rise ⁴	$Fukazawa^5$	Solea ⁶	$Panorama^7$	

1-(1),2-(2),3-(3),4-(6),5-(7),6-(8),7-(9)

References

- [1] B. A. Wing and J. M. Ferry, "Magnitude and geometry of reactive fluid flow from direct inversion of spatial patterns of geochemical alteration," *American Journal of Science*, vol. 307, no. 5, pp. 793–832, 2007.
- [2] L. Cathles, "An analysis of the hydrothermal system responsible for massive sulfide deposition in the Hokuroku Basin of Japan," *Economic Geology*, vol. Monograph 5, pp. 439–487, 1983.
- [3] D. Norton and H. Taylor Jr, "Quantitative simulation of the hydrothermal systems of crystallizing magmas on the basis of transport theory and oxygen isotope data: An analysis of the skaergaard intrusion," *Journal of Petrology*, vol. 20, no. 3, pp. 421–486, 1979.
- [4] R. Gregory, "Oxygen isotope history of seawater revised: timescales for boundary event changes in the oxygen isotope composition of seawater," *Stable isotope geochemistry: A tribute to Samuel Epstein*, vol. 3, pp. 65–76, 1991.
- [5] K. Muehlenbachs, "The oxygen isotopic composition of the oceans, sediments and the seafloor," *Chemical Geology*, vol. 145, pp. 263–273, 1998.
- [6] K. M. Gillis, K. Muehlenbachs, M. Stewart, T. Gleeson, and J. Karson, "Fluid flow patterns in fast spreading East Pacific Rise crust exposed at Hess Deep," *Journal of Geophysical Research: Solid Earth*, vol. 106, no. B11, pp. 26311–26329, 2001.
- [7] G. R. Green, H. Ohmoto, J. Date, and T. Takahashi, "Whole-rock oxygen isotope distribution in the Fukazawa-Kosaka Area, Hokoroku District, Japan and its potential application to mineral exploration," *Economic Geology*, vol. Monograph 5, pp. 395–411, 1983.
- [8] P. Schiffman and B. M. Smith, "Petrology and oxygen isotope geochemistry of a fossil seawater hydrothermal system within the Solea graben, northern Troodos ophiolite, Cyprus," *Journal of Geophysical Research: Solid Earth*, vol. 93, no. B5, pp. 4612–4624, 1988.
- [9] C. Brauhart, D. Huston, and A. Andrew, "Oxygen isotope mapping in the Panorama VMS district, Pilbara Craton, Western Australia: applications to estimating temperatures of alteration and to exploration," *Mineralium Deposita*, vol. 35, no. 8, pp. 727–740, 2000.